Chem., **34**, 131 (1972).
167. K. J. Vetter and J. W. Schultze, *ibid.*, **34**, 141 (1972).
168. V. S. Bagotskii, N. A. Shumilova, G. P. Samoilov, and E. I. Krushcheva, *Electrochim. Acta*, **17**, 1625 (1972).
169. B. E. Conway and E. Gileadi, *Trans. Faraday Soc.*, **58**, 593 (1962).
170. T. S. De Gromoboy and L. L. Shreir, *Electrochim. Acta*, **11**, 895 (1966).
171. L. M. Elina, T. I. Borisova, and T. I. Zalkind, *Zh. Fiz. Khim.*, **28**, 785 (1954).
172. A. C. Makrides, *This Journal*, **113**, 1158 (1967).
173. N. A. Shumilova and V. S. Bagotzky, *Electrochim. Acta*, **13**, 285 (1968).
174. A. I. Tsinman, *Elektrokhimiya*, **1**, 326 (1965).
175. Y. I. Turyan and A. I. Tsinman, *Zh. Fiz. Khim.*, **36**, 659 (1962).
176. A. Damjanovic, A. Dey, and J. O'M. Bockris, *Electrochim. Acta*, **11**, 791 (1966).
177. A. Damjanovic and J. O'M. Bockris, *ibid.*, **11**, 376 (1966).
178. A. Damjanovic and V. Brusic, *ibid.*, **12**, 615 (1967).
179. E. I. Krushcheva, N. A. Shumilova, and M. R. Tarasevich, *Elektrokhimiya*, **1**, 730 (1965).
180. L. Muller and L. N. Nekrasov, *J. Electroanal. Chem.*, **9**, 282 (1965).
181. L. Muller, *Electrochim, Acta*, **12**, 557 (1967).
182. M. R. Tarasevich and V. A. Bogdanovskaya, *Elektrokhimiya*, **7**, 1072 (1971).
183. A. V. Yuzhanina, V. I. Lukyanycheva, N. A. Shumilova, and V. S. Bagotskii, *ibid.*, **6**, 1054 (1970).
184. Ku. Ling-Ying, N. A. Shumilova, and V. S. Bagotskii, *ibid.*, **3**, 460 (1967).
185. D. T. Sawyer, and L. V. Interrante, *J. Electroanal. Chem.*, **2**, 310 (1961).
186. Yu. M. Tyurin and G. F. Volodin, *Elektrokhimiya*, **5**, 1203 (1969).
187. Yu. M. Tyurin and G. F. Volodin, *ibid.*, **6**, 1188 (1970).
188. Yu. M. Tyurin, G. F. Volodin, L. A. Smirnova, and Yu. V. Battalova, *ibid.*, **9**, 532 (1973).
189. D. Gilroy and B. E. Conway, *Can. J. Chem.*, **46**, 875 (1968).
190. J. L. Ord and F. C. Ho, *This Journal*, **118**, 46 (1971).
191. M. Ya. Fioshin and Yu. B. Vasilev, *Izv. Akad. Nauk SSSR, Otd. Khim. Nauk*, 437 (1963).
192. D. F. A. Koch and R. Woods, *Electrochim. Acta*, **13**, 2101 (1968).
193. A. K. Vijh and B. E. Conway, *Chem. Rev.*, **67**, 623 (1967).
194. P. R. Nadebaum and T. Z. Fahidy, *J. Appl. Electro-Chem.*, In press.

Electrochemical Oxidation of Ferrous Iron in Very Dilute Solutions

George B. Adams* and Roger P. Hollandsworth

Chemistry Department, Lockheed Missiles and Space Company, Incorporated, Palo Alto Research Laboratories, Palo Alto, California 94304

and Douglas N. Bennion*

Energy and Kinetics Department, School of Engineering and Applied Science, University of California, Los Angeles, California 90024

ABSTRACT

Experimental results are presented for the anodic oxidation of ferrous iron in dilute ferrous sulfate-sulfuric acid solutions. A conductive fixed-bed, flow-through, electrochemical reactor in which electric current flow is parallel to the direction of electrolytic solution flow was used. Steady-state anodic polarization curves were obtained at seven different flow rates, ranging from 1.5 to 10 ml/min in a cell of 81.1 cm^2 cross section. Input ferrous iron concentrations were 725 μg/ml in an acid mine water simulant containing 1430 μg/ml of sulfuric acid. Conversion efficiency for ferrous to ferric iron exceeded 99.9% at the lower flow rates. Design equations have been developed which predict performance of the system. Measured limiting currents exceed theoretical values by 6-14%. A preliminary cost analysis for a million gallons per day acid mine water treatment plant for oxidizing ferrous to ferric iron using parallel current-electrolytic solution flows predicts 7.5¢ per thousand gallons of which 4.6¢ per thousand gallons is assigned to capital costs. An additional 22.3¢ per thousand gallons must be added for following limestone treatment and precipitation of the ferric iron.

A serious industrial water pollution problem associated with coal mining operations results from the oxidation of iron pyrite in coal by exposure to air and water. This results in the formation of a dilute solution of ferrous sulfate and sulfuric acid, each product concentration varying typically from several hundred to several thousand micrograms/milliliter (acid mine water). To avoid pollution, this effluent must be neutralized and freed of iron before discharge into receiving waters.

A number of processes have been investigated for acid mine water treatment, including ion exchange, reverse osmosis, freezing, foaming, microbiological oxidation-limestone neutralization, ozone oxidation-limestone neutralization, and combination limestone-lime neutralization with aeration. Except for special circumstances, poor efficiencies, adverse economics, or both appear to rule out present use of most of these approaches. The principal treatment now in use commercially is the lime neutralization with aeration process.

An alternate approach is to preoxidize the ferrous ion electrolytically with subsequent iron precipitation and acid neutralization effected by addition of ground limestone. Certain economic advantages are claimed for this approach over the lime neutralization with

* Electrochemical Society Active Member.
Key words: ferrous oxidation, flow-through electrodes, water treatment.

aeration process (1-3). These previous studies report on processes in which electrolytic preoxidation was carried out in a conductive packed bed, flow-through reactor with current flow perpendicular to the direction of electrolytic solution flow. Maximum conversion efficiency for ferrous to ferric iron electro-oxidation of about 73% was achieved in the bench-scale reactor used. A rather complete mathematical analysis for that cell geometry has been presented by Alkire and Ng (4).

In the present work, a packed bed, flow-through reactor with powdered graphite filler was used with current flow parallel to the direction of electrolytic solution flow. Design and operation of this reactor, shown schematically in Fig. 1, is similar to that described by Bennion and Newman (5) and further tested by Wenger (6) and by Yip (7). The iron oxidation cell consists essentially of the anode half of the Bennion-Newman cell with a stainless steel cathode. Electrolytic solution was gravity-flowed through the cell, downward through the cathode screen, through a thick, porous anode, and then discharged through a micrometer control valve.

Design Principles

In order to achieve maximum utilization of the reactor volume, all or most of the volume must be involved in converting ferrous to ferric ions. The object is to maximize the average conversion rate per unit volume for the whole reactor and maintain product quality while minimizing the cost of the reactor and associated operating costs. The principal operating costs are electrical energy, pumping to overcome pressure drop across the cell, and associated labor and maintenance costs. Various geometries can be considered. However, this discussion is limited to the geometric cell configuration shown in Fig. 1 in which solution flow is parallel to electrical current flow and the counterelectrode is upstream of the working electrode. For this configuration, it has been shown (5, 6) that the pumping costs are very small. The details of labor costs are beyond the scope of this study. In the following calculations it is assumed that the system is capital intensive and that the primary objective is to achieve maximum conversion rates per unit volume. The effects of electrical energy costs on the design can be considered later. The basic principles used here are very similar to those presented earlier for a copper system (5).

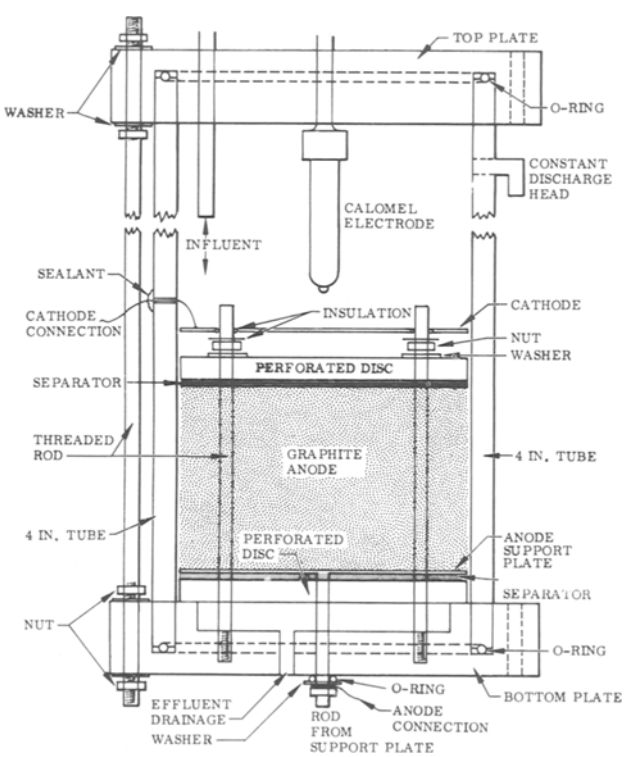

Fig. 1. Four-inch, flow-through electrolytic reactor

As fluid flows through the porous electrode, ferrous ions are transported from the bulk solution to the electrode surface and react to form ferric ions. The larger the electrode surface area per unit volume, a, the greater will be the reaction rate. It is assumed there is an excess of supporting electrolyte and that ferrous ions are transferred from bulk solution within the pores to the electrode surface by diffusion only. Thus the rate of reaction of the ferrous ions per unit area is proportional to the concentration difference between the bulk, c_b, and the surface, c_s. It is convenient to express the surface reaction rate in terms of the local transfer current density, j. Based on Faraday's law, the volumetric reaction rate, R, can be written as follows

$$R = \frac{aj}{\mathbf{F}} = ak_m (c_b - c_s) \quad [1]$$

k_m is the effective mass transfer coefficient. In order to maximize R, c_s must go to zero. This condition is achieved by applying a sufficiently large electrical potential driving force. The driving force must not be so large as to create excessive oxygen evolution.

Oxygen bubbles trapped in the packed bed will cause channeling and reduce the effective value of ak_m. The parameter combination ak_m is determined experimentally from the limiting current for ferrous to ferric conversion prior to O_2 evolution. Electrolytically evolved oxygen or other oxidant diffusing into the bulk of a pore and oxidizing ferrous iron in the pore leads to values of j larger than predicted by Eq. [1] based on ferrous diffusion only. This latter effect will be dominant in early stages of oxygen evolution, but, as oxygen bubbles continue to plug the bed more and more, the effects of oxygen evolution can decrease over-all performance.

A material balance on the ferric ion yields the concentration distributed within the flow-through porous electrode

$$v \frac{dc_b}{dy} = -R = -ak_m c_b \quad [2]$$

The symbols are defined at the end of the paper. The variation of the potential driving force is described by Ohm's law and the conservation of charge

$$i = \kappa \frac{d\phi}{dy} \quad [3]$$

$$aj = \frac{di}{dy} \quad [4]$$

i is the superficial or observed current density and κ is an effective, electrolytic conductance in the porous bed.

The boundary conditions are

$$c_b = c_o \text{ at } y = 0 \quad [5]$$

$$i = 0 \text{ at } y = L \quad [6]$$

$$\phi = 0 \text{ at } y = L \quad [7]$$

$$c_b = c_L \text{ at } y = L \quad [8]$$

The final condition is not really a boundary condition, but more of a design criterion. Given c_L, the optimum electrode thickness, L, and flow rate, v, can be determined. The solution to these equations is

$$c_b = c_o \exp(-\alpha y) \quad [9]$$

$$i = Fvc_o [\exp(-\alpha y) - c_L/c_o] \quad [10]$$

$$\Delta\phi = \beta[\exp(-\alpha y) - 1 + \alpha y c_L/c_o] \quad [11]$$

where

$$\alpha = ak_m/v \quad [12]$$

$$\beta = Fv^2c_o/ak_m\kappa \quad [13]$$

As a first approximation, the cost of a processing plant will depend on the volume or weight of cells required to process a given feed flow rate of acid mine waters to be treated. The volume of cells is just the area, A, times the thickness, L. The area, A, is the feed flow rate, F, in cm^3/sec divided by the maximum allowable feed velocity through the cell, v

$$A = F/v \quad [14]$$

The larger the velocity v, the smaller A, and the lower the capital cost. Typically k_m depends on the velocity through the bed and the bed geometry expressed through the area per unit volume, a, and the particle shape factor, ψ. A correlation suggested by Bird *et al.* (8) has been used

$$\frac{k_m}{aD} = 0.91\frac{\rho v^{0.49}}{a\mu\psi}\psi^2Sc^{1/3} \quad [15]$$

Given c_o, c_b^L, a, $\Delta\phi$, and κ, Eq. [9], [11], and [15] can be solved for v, L, and κ_m. Equation [15] assumes no channeling. If there is channeling, one must use an effective a which may be much smaller than the geometric a based on particle size alone. The larger the magnitude of $\Delta\phi$, the larger will be v. L also increases with $\Delta\phi$, but the gain in v more than offsets any increased size associated with the larger L. The larger the magnitude of $\Delta\phi$, the greater the rate of oxygen evolution. A value of about -1.7V appeared optimum for the experiments reported on here. For higher magnitude $\Delta\phi$, the oxygen which formed caused channeling which reduced the effective value of a and thus v_{max} decreased with further increase in magnitude of $\Delta\phi$. The optimum value of $\Delta\phi$ could vary considerably with local operating conditions.

The effective electrolytic conductivity in the porous electrode, κ, was estimated using the Bruggemann equation (9, 10)

$$\kappa = \kappa_o\epsilon^{1.5} \quad [16]$$

where κ_o is the bulk electrolytic solution conductivity and ϵ is the porosity of the electrode.

Given c_o, c_b^L, L, v, and κ from experimental observations, it is possible to calculate effective values of $\Delta\phi$, a, and k_m. If the effective a is much smaller than a calculated from the geometric area of the packing material, it implies there is channeling of the flow through the bed. It was not possible to measure $\Delta\phi$ directly. However, by placing a reference electrode in the effluent stream and measuring its potential relative to the anode, one measures a potential V_p. This V_p is essentially $\Delta\phi$ plus any electronic resistance losses in the matrix, surface overpotential at the front of the electrode, local concentration overpotential at the front of the electrode, and possibly a constant term which depends on the particular reference electrode selected. These local effects in comparing V_p and $\Delta\phi$ have been discussed by Wenger (6). It seems sufficient to state here that V_p is related to $\Delta\phi$. The larger V_p, the larger the magnitude of $\Delta\phi$ and the greater the tendency for oxygen evolution.

In experimental runs, current is increased by increasing the cell voltage, V_f, and measuring V_p. When limiting current is reached throughout the cell, c_s everywhere very much less than c_b, further increases in the cell voltage increase V_p, but the current no longer changes. The length of the I *vs.* V_p plateau is a measure of the excess capacity of the cell. As v is increased, the length of the limiting current plateau decreases. When the plateau just disappears with increasing v, the maximum velocity is assumed to have been established experimentally, see Fig. 2 and 3. For a given set of input and output conditions, the larger the value of the effective a, the larger will be the maximum v. Thus the importance should be clear of minimizing channeling and realizing an effective a as close to the geometric or true a as possible.

Experimental

Cell construction.—The experimental reactor is shown in Fig. 1. It is constructed of Plexiglas tubing, 4 in. ID, with two end plates consisting of Plexiglas disks fitted with O-rings to close off both ends of the tube. Sealing is effected by compression of six external, threaded, steel rods located peripherally on the end plates at 60 degree intervals. The graphite bed is contained between two Plexiglas support plates containing 72 ¼-in. and 18 ⅜-in. perforations spaced in a geometrical pattern to give a uniform flow rate and still maintain structural strength. These support plates are compressed by means of six internal stainless steel threaded rods. Cloth separators, placed below the top perforated support plate and below the perforated anode support plate, prevent graphite particles from washing out of the bed by the electrolytic solution flow. The graphite used in the bed was Stackpole Carbon Company, Grade 6026 graphite, sized to $-100 + 150$ mesh.

Electrical circuit.—Circuitry was similar to that used by Bennion and Newman (5). Influent and effluent were monitored continuously for *p*H and conductance. Anode potential was measured *vs.* saturated calomel reference electrodes located above the cathode (V_f) and below the anode (V_p) in the effluent stream. Conductance was measured with Beckman flow-through conductivity cells (cell constant 0.5 cm^{-1}). Anode potential, cell voltage, and *p*H were measured with an Orion Model 601, digital *p*H meter; cell resistance was measured with a General Radio tube 1650-A impedance bridge. Power was supplied to the cell from a Gerhard Bark, Wenking potentiostat in which the impressed current is regulated at a constant potential between anode and a calomel reference electrode placed above the cathode (V_f).

Flow control.—Flow of effluent being discharged was controlled with a Nulcear Products Company micrometer valve. Influent flow rate was adjusted always to exceed that of the effluent, the overflow being discharged through an outlet located near the top of the reactor in order to maintain a constant head of electrolytic solution on the micrometer valve exit port. This was necessary in order to minimize fluctuations in flow rate over 24 hr periods. Flow rates were determined using graduated cylinders to collect known volume of effluent over measured time intervals.

Electrolyte concentrations.—The electrolytic solution was an acid mine water simulant, 725 μg/ml in ferrous iron (as ferrous sulfate heptahydrate) and 1430 μg/ml in H_2SO_4. Solutions were made up from deionized water and reagent grade (J. T. Baker) chemicals. The *p*H of the influent electrolyte ranged from 1.9 to 2.1 with a mean conductivity of 0.065 mho/cm. Influent temperature varied between 22° and 26°C.

After reaching a steady state for V_p at each V_f setting for a given flow rate, the effluent was analyzed for the ferrous and total iron concentration. Analysis was made spectrophotometrically, using a Beckman Model D2 spectrophotometer. Either 1-10 phenanthroline or α-α' bipyridyl procedures were followed (11), depending on the ferrous iron concentration.

For solutions containing less than 10 μg/ml of ferrous iron, two parts (by volume) of the sample were diluted by addition of one part of saturated potassium fluoride solution to complex ferric ions, thereby inhibiting formation of the colored ferric complex. An additional one part of α-α' bipyridyl solution (2% in 6*N* HCl) was then added to form the yellow ferrous complex which was determined spectrophotometrically at 415 mμ. For solution containing more than 10 μg/ml ferrous iron, the sample was suitably diluted to give 0-3 μg/ml, and the red 1-10 phenanthroline ferrous complex was determined at 515 mμ. Total iron was determined by using a 500× dilution treated with solid hydroxylamine hydrochloride to reduce ferric to fer-

rous iron, followed by spectrophotometric determination of the red O-phenanthroline complex.

Above 20 μg/ml, accuracy of the analytical determinations was about 7%; at the lower limit of the measurements near 1 μg/ml, the accuracy was 10%.

Materials compatibility.—It was found necessary to thickly gold plate 316 stainless steel anode support plate and the six internal tie rods, washers, and nuts. All other metal exposed to the electrolyte was unplated 316 stainless steel. The cell body was Plexiglas. Separators were cut from Webril material, a nonwoven Dacron cloth.

Results

Figures 2 and 3 show the family of anodic polarization curves (I *vs.* V_p) at seven flow rates ranging from 1.5 to 10 ml/min, or 3.1×10^{-4} to 2.1×10^{-3} cm/sec. These results were obtained under steady-state conditions with an electrolytic solution of acid mine water simulant containing from 705 to 725 μg/ml ferrous iron. Runs were made at constant flow rate. Variations in flow rate of up to 10%, in some cases, occurred due mainly to temperature variations occurring overnight with consequent viscosity changes in the solution. Flow rates for each point have been normalized to the value shown for each curve and the corresponding current values corrected accordingly. From 4 to 24 hr are required to reach a true steady state for each point on the curve after each change in the control potential V_f. Superficial residence time is of the order of 8 hr. It normally takes about three superficial residence times to achieve a steady state. This point is discussed in greater detail by Bennion and Newman (5) in their work on copper deposition. Shapes of the curves are typical (at flow rates up to 6.85 ml/min) for an electrode process approaching and then establishing a limit current. A reasonably identifiable plateau is established before the rapid rise due to oxygen evolution occurs.

Analysis of the effluent stream for ferrous and total iron concentrations was carried out for each run. Coulombic conversion efficiencies of over 99.9% were obtained at the lower flow rates. Effluent ferrous iron concentration is given in micrograms/milliliter beside each datum point. Effluent total iron concentration was lowered from that of the influent by electrodeposition of some metallic iron at the cathode.

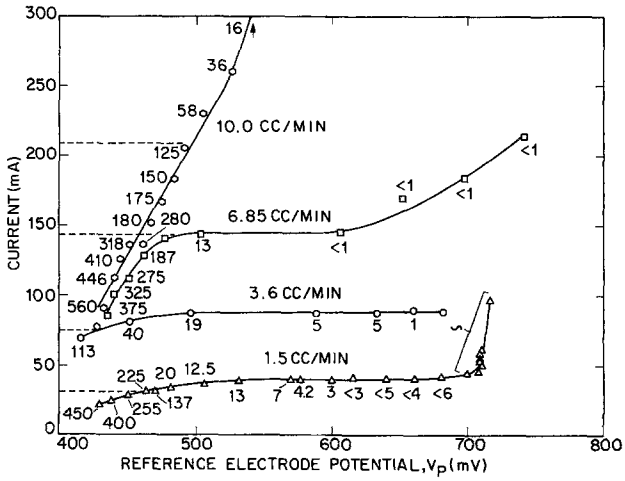

Fig. 2. Polarization curves for porous, flow-through anode. 81.1 cm^2 cross section, 7.4 cm length, $\kappa_{in} = 6.5 \times 10^{-3}$ mho/cm, $\kappa_{out} = 5.3 \times 10^{-3}$ mho/cm, $Fe^{++}{}_{in} = 725$ ppm, $Fe^{++}{}_{out}$ noted by numbers next to experimental points. Average total iron out = 705 ppm. Flow rate noted beside each curve. - - - - shows calculated limiting currents.

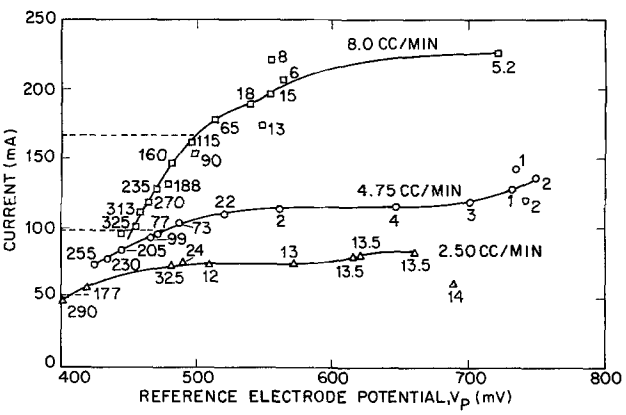

Fig. 3. Polarization curves for porous, flow-through anode. Conditions same as for Fig. 2, only for different flow rates.

Discussion

Current increment.—Table I is a summary of steady-state, limiting current operation at various flow rates. Comparing the calculated current based on Eq. [10] and the observed current shows the observed current to be consistently 10-12 mA higher. This effect is also shown by comparing the dashed lines and plateau positions in Fig. 2 and 3. One possible explanation of this difference is that hydrogen produced at the cathode and dissolved in the electrolyte is oxidized in the bed to give the observed increment of current. It is difficult to account for more than half this difference, however, assuming the solution is saturated (not supersaturated) with hydrogen at a solubility concentration of 1.34 ppm. An experiment was conducted at 1.50 cm^3/min to test this concept using a Nafion XR-475 ion exchange membrane to separate the dissolved hydrogen formed at the cathode from the anode bed. No decrease in limiting current was observed. This experiment supports the view that the anomalous current increment is not due to electro-oxidation of hydrogen.

Another point mitigating against the concept of oxidation of dissolved hydrogen is that the incremental current observed should increase with increasing flow rate for any dissolved species being oxidized. This does not occur; the incremental current remains essentially constant at about 10-12 mA.

Another explanation of the anomalously high observed limiting current and the relatively constant value of the current increment at increasing flow rates is that the incremental current is due to the anodic oxidation of the graphite surface. Since the oxidation product may be a solid and remain on the surface of

Table I. Analysis of operating conditions

Electro-oxidation of Fe^{++} to Fe^{+++}, $e = 0.5$, $A = 81.073$ cm^2, $Sc = 1366$, $\kappa^\circ = 5 \times 10^{-8}$ mho/cm.

Input data				Calculated values			Other observed data		
L, cm	Flow, cm^3/min	c_L, μg/ml	c_o, μg/ml	a, cm^{-1}	$-\Delta\phi$, V	I, mA	I, mA	V_p, mV	V_f, mV
7.4	1.46	0.6	695	8.89	0.212	29.2	41.2	−681	−996
7.4	2.23	1.35	705	9.47	0.368	45.2	62.0	−616	−1025
7.4	3.64	0.5	725	12.36	0.536	75.9	87.8	−633	−1175
7.4	4.75	0.4	775	13.87	0.720	105.9	115.8	−647	−1398
7.4	6.90	0.1	755	17.56	0.866	150.0	146.0	−606	−1496
7.4	8.14	6.0	725	12.30	1.742	168.5	211.0	−564	−1801
7.4	9.25	58.0	760	12.99	2.048	200.9	213.0	−506	−1799

the graphite, no dissolved species would be involved, and hence no increase in incremental current with flow rate would occur. A recent study (12) has shown that hydroquinone-like groups on a graphite surface are anodically oxidized to quinone-like groups. These quinone-like surface species could eventually react with the ferrous ions to establish a steady-state condition. Other observations favoring this point are that the bed appeared to improve with age, and that a yellow colloidal layer appeared above the packed graphite bed when the reactor was back flushed after running above oxygen evolution potentials for a prolonged period. Quinoidal compounds are usually colored.

If carbon is reacting, eventually the carbon bed will be destroyed. Over a three month period of operation, the graphite bed used in these experiments showed no noticeable deterioration. If impurities in the graphite are involved, eventually they would be used up and the excess current would no longer be observed. If the impurity level is estimated at 5% of the graphite by weight and to have an effective equivalent weight of 50, a graphite bed of 700g would contain 0.7g equivalents of impurities. Assuming operation for 20 days at 10 mA excess current implies consumption of only 0.18g equivalents in some Faradaic reaction other than ferrous iron oxidation. (This calculation is only good to about an order of magnitude.) Hence, it is concluded that for the length of time involved, impurities could have been reacting or possibly graphite breakdown would not have been extensive enough to be noticed.

Another more obvious explanation for the excess current is oxygen evolution. If bubbles of oxygen form, they are expected to plug the porous electrode flow channels and cause electrolyte channeling, which should result in poor iron oxidation rates. Since observed oxidation rates were high, it could be that oxygen did not nucleate, but reacted with ferrous iron as fast as it formed at the graphite surface. It is known that the uncatalyzed reaction of molecular oxygen with ferrous iron is a slow reaction (13). However, this reaction is catalyzed by activated carbon (14). Hence, the rapid oxidation of ferrous iron by the active oxygen forming in the bulk of the electrode pores cannot be ruled out.

A difficulty with both the quinone and oxygen evolution explanations for the anomalous limiting current increment is that the anomaly is observed at potentials below those required for either oxygen evolution or surface quinone formation.

It seems improbable that peroxide, formed by partial oxidation from water, could be the active intermediary, since at pH 2 the oxidation of ferrous iron by hydrogen peroxide is incomplete unless a large excess of peroxide is present.

The experimental results presented here are not sufficient to determine the precise secondary reaction or reactions taking place. However, the results do indicate that electrochemical oxidation of ferrous ions is feasible and that the proposed design equations and procedures work and yield conservative design conditions. The unaccounted for side reactions apparently do not hinder operation so far as has been determined to date. Their possible beneficial effects should not be counted upon until more is known about them and under what conditions they occur.

Conversion efficiency.—As shown in Fig. 2, conversion efficiency of ferrous to ferric iron is over 97% at the highest flow rate (10 cm^3/min), the last point indicated on the curve. This high conversion efficiency is achieved even though no limiting current is established at this high flow rate. Normally one would expect a relatively low conversion efficiency under these conditions, since ferrous iron flows through the bed faster than it can diffuse to the anodic surfaces and be oxidized. Surface quinone formation at the anode, as discussed above, could serve as a solid redox couple and catalyze the oxidation of ferrous ion, especially if it were partially soluble in the electrolyte. In effect, it would increase the effective mass transport coefficient of ferrous ion by rapidly oxidizing it within the pores of the graphite anode surface.

Cost analysis.—Using actual data at a cell flow rate of 8.14 cm^3/min, feed of 725 μg Fe^{++}/ml, feed conductivity of 0.005 mho/cm, effluent concentration of 6 μg Fe^{++}/ml, bed length of 7.4 cm, and a bed shape factor of 0.86 yields an effective surface area per unit volume for the bed of 12.3 cm^{-1} and an allowable resistance loss through the bed of 1.768V. The effective surface area is quite low compared to an estimated geometric specific surface area of over 100 cm^{-1}. By optimizing the packing material to get more uniform size distribution, the specific surface can probably be increased substantially, possibly to between 26 and 50 cm^{-1}. For design estimates here, specific area of 14 cm^{-1} and 1.7V resistance potential drop across the packed bed will be used. In order to compare costs with previous estimates (3), feed of 500 μg Fe^{++}/ml and effluent with 95% conversion[1] (25 μg Fe^{++}/ml) will be used as the design basis. These conditions imply an optimum bed length of 4.8 cm and a flow velocity of 2.7×10^{-3} cm/sec or 57 gal/day·ft^2. To take advantage of any soluble oxidant or dissolved oxygen production in the cell, the cell should be made a little longer than 4.8 cm, possibly up to 7 cm.

To handle one million gallons per day, the above cell design implies that 17,544 ft^2 of cell area will be needed. If the cells are coated concrete slabs and walls with a packed bed on top, a separator, a cathode, the concrete container filled with electrolytic solution, and a hood to collect the hydrogen, the construction cost is assumed to be similar to that of a concrete slab warehouse for which the construction cost is estimated (15) as \$9.50/ft^2. Detailed cost estimating procedures for copper removing flow-through electrodes yield \$4 to \$15/ft^2, depending on design details and cost bases. It seems reasonable to assume a cost of \$10/ft^2 for a large-scale reactor of this type.

At \$10/ft^2, the cost of a one million gallon per day reactor will be \$175,440. For purposes of comparison, straight line depreciation over ten years with no interest charges is assumed. This gives a fixed cost of \$17,544 per annum or 4.8¢ per thousand gallons of acid mine water treated. For cell voltage of 3V, it requires 2.73 kW-hr to treat one thousand gallons of feed assuming 100% current efficiency for the $Fe^{++} \rightarrow Fe^{+++} + e^-$ reaction. If power costs 1¢/kW-hr, energy costs will be 2.7¢ per thousand gallons of feed. Other costs for limestone precipitation have been estimated (3) to be 22.3¢ per thousand gallons based on 500 μg Fe^{++}/ml and 1000 μg/ml total acidity. This implies a total treatment cost of 29.8¢ per thousand gallons. This cost figure compares to 36¢ per thousand gallons for the Tyco Laboratories estimate (3). A credit of 6¢ per thousand gallons for salable hydrogen gas produced is deductible from each of these figures for comparison with nonelectrolytic processes. Sludge handling costs are not included in these estimates.

Cost estimates of this type are of necessity approximate. They should be useful for preliminary comparisons and to illustrate how the costs are capital intensive at today's energy costs. By achieving higher flow rates per unit geometric area and/or lower cost per unit geometric area of the electrode, more favorable economic situations should be possible. In particular, larger values of the effective specific surface area, a, should allow for higher flow rates. This might be achieved by minimizing channeling of electrolytic solution flow through the bed and increasing the actual specific surface area within the bed.

Other applications.—This use of flow-through, porous electrode reactors should be applicable to the anodic oxidation of cyanide ions from dilute solutions

[1] This is reported to be (3) the lowest conversion efficiency for Fe^{++} that will allow complete precipitation of iron by addition of limestone.

such as plating rinse waters for cyanide concentrations up to several hundred parts/million. It should also be applicable to the reduction of chromate to chromic ions in plating bath rinse waters from acid chromium plating baths. In addition it should be possible to cathodically strip gold, silver, copper, and nickel from plating bath rinse waters. The details for metal recovery are discussed elsewhere (5, 6, 16). By using a combination of cyanide destruction and ion recovery, it may be possible to clean rinse waters for reuse.

Acknowledgment

This research was supported as part of the 1973 Lockheed Independent Research Program.

Manuscript submitted Nov. 8, 1974; revised manuscript received April 1, 1975.

Any discussion of this paper will appear in a Discussion Section to be published in the June 1976 JOURNAL. All discussions for the June 1976 Discussion Section should be submitted by Feb. 1, 1976.

Publication costs of this article were partially assisted by Lockheed Missiles and Space Company, Incorporated.

SYMBOLS

- a specific surface area, cm^{-1}
- A geometric cross sectional flow channel area, cm^2
- c_b bulk ferrous ion concentration in pores, mol/cm^3
- c_L effluent ferrous ion concentration, mol/cm^3
- c_o influent ferrous ion concentration, mol/cm^3
- c_s ferrous ion concentration at surface of pore walls, mol/cm^3
- D diffusion coefficient of ferrous ions, cm^2/sec
- $\mathbf{F}$ Faraday constant, 96,487 coulombs/equiv.
- i superficial or geometric current density, A/cm^2
- I total current, A
- j transfer current density across pore walls, A/cm^2
- k_m mass transfer coefficient, cm/sec
- L length of porous anode, cm
- R effective reaction rate per unit volume within anode, $mol/cm^3 \cdot sec$
- Sc Schmidt number, $\mu/\rho D$
- v superficial fluid velocity, cm/sec
- V_f potential of a saturated calomel reference electrode in feed solution relative to anode, V
- V_p potential of a saturated calomel reference electrode in effluent solution relative to anode, V
- y distance along porous anode in direction of flow, cm
- α ak_m/v, cm^{-1}
- β $\mathbf{F}v^2 c_o/ak_m\kappa$, V
- ϵ void fraction, dimensionless
- κ effective or superficial electrical conductivity of catholyte, mho/cm
- μ viscosity of feed solution, $g/cm \cdot sec$
- ρ density of feed solution, g/cm^3
- ϕ potential in solution, V
- $\Delta\phi$ potential drop in solution across porous electrode, V
- ψ particle shape factor, 0.86 for flakes, dimensionless

REFERENCES

1. Bituminous Coal Research, Inc., E.P.A. Report, Water Pollution Control Research Series DAST-33, 14010 E1Z61/70 (Jan. 1970).
2. Bituminous Coal Research, Inc., E.P.A. Report, Environmental Protection Technology Series, 14010 EZ12/71 (Dec. 1971).
3. Tyco Laboratories, Inc., E.P.A. Report, Water Pollution Control Research Series, 14010 FNQ 02/72 (Feb. 1972).
4. Richard Alkire and P. K. Ng, *This Journal,* **121,** 95 (1974).
5. D. N. Bennion and John Newman, *J. Appl. Electrochem.,* 2, 113 (1972).
6. R. S. Wenger, M.S. Thesis, School of Engineering, Univ. of California, Los Angeles (Feb. 1974).
7. H. K. Yip, M.S. Thesis, Chemical Engineering Dept., Univ. of California, Berkeley (June 1973).
8. R. B. Bird, W. E. Stewart, and E. N. Lightfoot, "Transport Phenomena," John Wiley & Sons, Inc., New York (1960).
9. R. E. de la Rue and C. W. Tobias, *This Journal,* **106,** 827 (1959).
10. D. A. G. Bruggemann, *Ann. Physik.,* **24,** 636 (1935).
11. W. M. Banick, Jr. and G. F. Smith, *Talanta,* **1,** 153 (1958). Also "Standard Methods for Examination of Water and Wastewater," 12th Ed., p. 156, (1965), prepared and published by A.P.H.A., A.W.W.A., and W.P.C.F.
12. K. F. Blurton, *Electrochemica Acta,* **18,** 869 (1973).
13. Harvard University, Water Pollution Control Research Series 14010-06/69, Water Quality Office, U.S. Environmental Protection Agency, Washington, D. C.
14. C. T. Ford and J. F. Royer, Environmental Protection Technology Series, EPA-R2-73-150 (Jan. 1973), Office of Research and Monitoring, U.S. Environmental Protection Agency, Washington, D. C.
15. "The National Construction Estimator," 18th ed. p. 174, Craftsman Book Co., Solana Beach, Calif. (1970).
16. D. N. Bennion and John Newman, U.S. Pat. 3,804,733 (April 16, 1974).